Lab on a Chip

View Online
Dynamic Article Links

Cite this: *Lab Chip*, 2011, **11**, 2189

www.rsc.org/loc

PAPER

Paper-based piezoresistive MEMS sensors†

Xinyu Liu,[a] Martin Mwangi,[a] XiuJun Li,[a] Michael O'Brien[a] and George M. Whitesides*[ab]

Received 24th February 2011, Accepted 11th April 2011
DOI: 10.1039/c1lc20161a

This paper describes the development of MEMS force sensors constructed using paper as the structural material. The working principle on which these paper-based sensors are based is the piezoresistive effect generated by conductive materials patterned on a paper substrate. The device is inexpensive (~$0.04 per device for materials), simple to fabricate, lightweight, and disposable. Paper can be readily folded into three-dimensional structures to increase the stiffness of the sensor while keeping it light in weight. The entire fabrication process can be completed within one hour without expensive cleanroom facilities using simple tools (*e.g.*, a paper cutter and a painting knife). We demonstrated that the paper-based sensor can measure forces with moderate performance (*i.e.*, resolution: 120 μN, measurement range: ±16 mN, and sensitivity: 0.84 mV mN^{-1}). We applied this sensor to characterizing the mechanical properties of a soft material. Leveraging the same sensing concept, we also developed a paper-based balance with a measurement range of 15 g, and a resolution of 0.39 g.

Introduction

The past three decades have witnessed the extensive development of MEMS (Micro-Electro-Mechanical Systems) devices and systems, which have found important applications in industry and medicine.[1–4] Examples of commercially successful MEMS products include digital micromirror devices (DMD, Texas Instruments), accelerometers for triggering air bags in automobiles (Analog Devices and Motorola), and pressure/flow sensors for industrial uses (Honeywell).

Silicon-based materials (*e.g.*, single crystal silicon, polycrystalline silicon, silicon dioxide, and silicon nitride) are the primary materials used for constructing MEMS devices, and manufacturing approaches are derived from microfabrication processes developed for integrated circuits (ICs).[5] The microfabrication process as used for silicon-based MEMS (especially for prototyping) is time-consuming (days for a single batch) and requires access to cleanroom equipments. Both materials and use of cleanroom are expensive; and although the performance of silicon-based MEMS can be excellent, their relatively high cost has limited the applications they can address.

We are interested in the development of new MEMS technologies, where the emphasis is on minimizing cost, and the ratio of performance to cost is maximized by minimizing cost rather than maximizing performance. We have chosen paper as the material to serve as the basis for this exploratory progress. A conceptually related effort to reduce the cost of diagnostic systems by developing paper-based diagnostic systems has developed into a new approach to diagnostic technologies.[6–11] Paper is readily available, lightweight, and easy to manufacture; the paper substrate makes integration of electrical signal-processing circuits onto the paper-based MEMS devices straightforward. As our first investigation of paper for the construction of MEMS, we developed a paper-based piezoresistive force sensor, and applied it to mechanical characterization of soft materials. We also demonstrated a paper-based weighing balance. These paper-based MEMS devices have characteristics (*e.g.*, low cost, portability, and easy disposability) appropriate for single-use sensors in analytical applications (*e.g.*, mechanical characterization of tissues in medical diagnostics, and measurement of viscosity of foods, such as mayonnaise and meringue gels, and non-Newtonian fluids).

Experimental design

Working principle of the paper-based force sensors

The sensing principle of the paper-based force sensor is the piezoresistive effect of conductive materials patterned on a paper structure (a cantilever beam in this work). Many MEMS sensors (including commercial devices) also take advantage of the piezoresistive effect, but are typically constructed from silicon-based semiconductor materials. Instead, we used paper as a structural material for construction of the devices; paper is much cheaper (*e.g.*, $0.1 per m^2 for printing paper) than silicon, and provides other advantages (*e.g.*, light weight, disposability, and ease of manufacturing) over silicon.

[a]*Department of Chemistry and Chemical Biology, Harvard University, Cambridge, MA, 02138, USA. E-mail: gwhitesides@gmwgroup.harvard.edu*
[b]*Wyss Institute for Biologically Inspired Engineering, Harvard University, Cambridge, MA, 02138, USA*
† Electronic supplementary information (ESI) available. See DOI: 10.1039/c1lc20161a

Fig. 1A shows a schematic diagram of a simple, paper-based force-sensing cantilever. In this device, a carbon resistor is located at the root of the cantilever, where the maximum surface strain occurs during deflection. We designed the carbon resistor to be short (7 mm) relative to the length (44.5 mm) of the cantilever. When a force is applied to the beam structure, the resistor experiences a mechanical strain/stress, which then induces a change in resistance of the resistor. Measuring the change in resistance allows quantification of the applied force.

Device fabrication

Fig. 1B summarizes the process used to fabricate the device. We fabricated paper cantilever beams by cutting Whatman® 3MM chromatography paper (340 μm thick, 186 g m^{-2}) using a laser cutter. The precision of laser cutting was 0.1 mm. The length and width of the cantilever beam were 44.5 ± 0.1 mm and 7.7 ± 0.08 mm, respectively. We screen-printed carbon resistors using high-resistivity graphite ink, and contact pads using low-resistivity silver ink. Fabricating an array of paper-based force sensors (Fig. 1C) typically takes less than one hour.

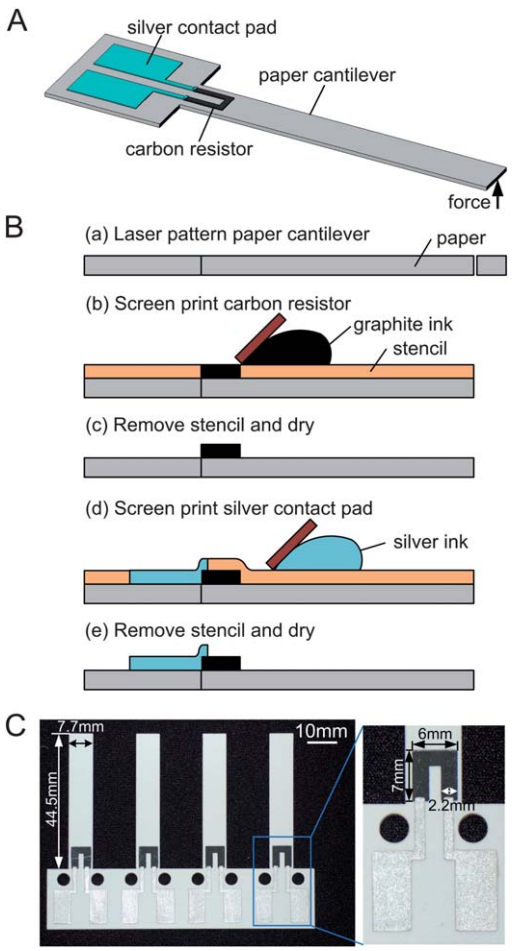

Fig. 1 Paper-based piezoresistive force sensor. (A) Schematic view of a paper-based force sensor using a carbon resistor as the sensing component. (B) Fabrication process of the paper-based sensor involving laser cutting of paper and screen printing of carbon and silver inks. (C) A photograph of an array of four devices with labeled dimensions.

Paper is hydrophilic, and adsorption of water, with resultant changes in mechanical and electrical properties of the sensor, is a potential concern. To render the paper hydrophobic, we functionalized the surface hydroxyl groups of the paper (cellulose fibers) with (tridecafluoro-1,1,2,2-tetrahydrooctyl) trichlorosilane vapor to form surface silanol linkages, and thus generated a fluorinated, highly textured, hydrophobic surface. This surface treatment minimizes the effect of environmental humidity on the mechanical and electrical properties of the sensor. The contact angle of water on the silanized paper substrate was 140° (for comparison, contact angles of water on polyethylene and Teflon films are 100° and 120°, respectively[12,13]).

Results and discussion

Mechanical properties of paper cantilever beams

We first characterized the stiffness of the paper cantilever beams using a precision balance (model EP64, Ohaus Explorer Pro, Fig. S1†; force measurement resolution: 0.98 μN), by measuring forces applied to the free end of a paper cantilever as a function of the beam deflections. Fig. 2A shows force–deflection data based on measurements of seven devices. The stiffness of a paper cantilever (44.5 mm long, 7.7 mm wide, and 0.34 mm thick) was determined to be 2.0 ± 0.16 mN mm^{-1} (mean ± one standard deviation). By choosing different types of paper with different compositions and thicknesses, the stiffness of the paper

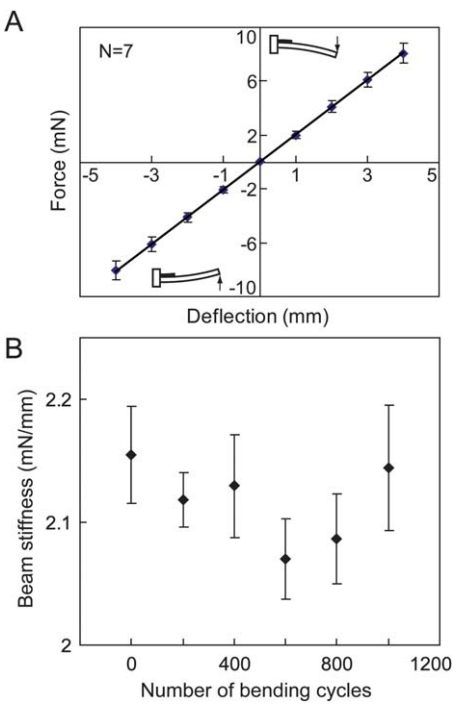

Fig. 2 Mechanical properties of paper cantilever beams. (A) Calibration plots of force–deflection data based on the measurements of seven devices. The schematic insets illustrate the types of mechanical strains (stretching *vs.* compressive) applied to the carbon resistors. The solid line represents a linear fit to the force–deflection data with a regression equation: $y = 2.0x$ ($R^2 = 0.9999$, $N = 7$). (B) Experimental data of beam stiffness as a function of the number of repeated bends.

cantilever (with the same dimensions) can be readily tuned in a wide range (see Table S1† for values of stiffness of the cantilevers with the same dimensions, but made from different types of paper).

We also tested the mechanical reliability of the paper device through repeated bending of a cantilever beam up to 1000 times. After every 200 cycles of bending, we tested the force–deformation curves for the paper cantilever seven times, and calculated the average beam stiffness based on the data from the seven measurements. Fig. 2B shows data characterizing beam stiffness as a function of the number of bends. The change of the beam stiffness during the 1000 cycles of bending is <4%. These data demonstrate stable mechanical properties (stiffness) of the paper cantilever beams, and suggest that silanized (hydrophobized) paper is a suitable structural material for constructing MEMS devices.

To compare the stiffness of paper with that of other materials for constructing MEMS devices, we estimated the Young's modulus of the paper beam, based on the data of force–deformation curves (Fig. 2A). We calculated the Young's modulus of the paper using a beam equation (eqn (1)), with the assumption that paper is a solid and homogeneous material:

$$E = \frac{4FL^3}{\delta WH^3} \quad (1)$$

Here, E is the Young's modulus (in kPa) of the paper, F is the force (in mN) applied to the free end of paper beam, δ is the deflection (in mm) of paper beam, and L, W, and H are length, width, and thickness (in mm) of the beam respectively. The Young's modulus of the paper was determined to be 2.0 ± 0.17 GPa ($N = 7$), which is approximately 66 to 86 times lower than that of silicon (130–170 GPa for single crystal silicon).[5] We are aware that, because paper is porous, the value of Young's modulus that we calculated is not the Young's modulus of cellulose itself (fibers of which form the paper), but an equivalent to Young's modulus for the paper in the format of a porous sheet.

Electrical properties of carbon resistors

We measured the current–voltage (I–V) characteristic of the carbon resistor using a source meter (Keithley 2400). All the measured resistors ($N = 7$) revealed a linear, ohmic I–V behavior (Fig. 3A), suggesting that the piezoresistivity of the carbon resistor correlates primarily with the strain-induced shape deformations of the resistor. The resistance of the resistors we tested was 600 ± 190 Ω ($N = 7$).

We also investigated the temperature coefficient of resistance of the carbon resistors. This coefficient is defined as the ratio of relative change in resistance of a resistor ($\Delta R/R_0$) to the change in temperature (ΔT). Fig. 3B shows the relative change in resistance of the carbon resistors as a function of the change in temperature. These data yield a temperature coefficient of resistance of 0.0012 ± 0.0007 per °C ($N = 7$). The effect of temperature on the output of the sensor could, in principle, be cancelled by laying out another carbon resistor on the cantilever for temperature compensation and integrating it into the circuit for signal readout (*i.e.*, in a Wheatstone bridge circuit, or some equivalent circuit).

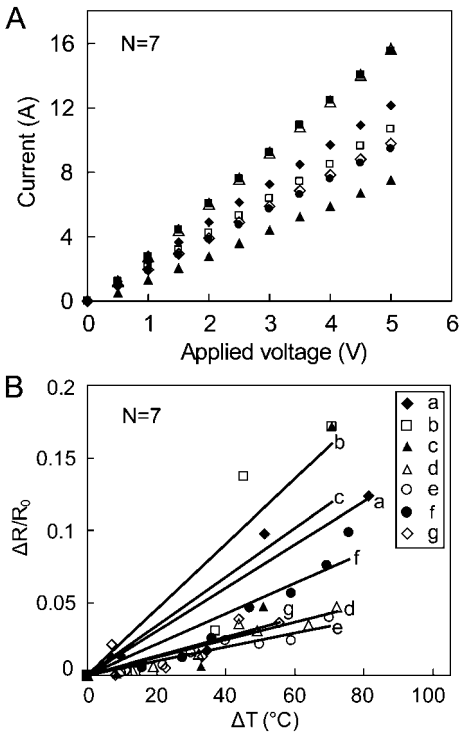

Fig. 3 Electrical properties of carbon resistors. (A) Linear current–voltage curves for carbon resistors ($N = 7$), showing the ohmic I–V characteristics of a good conductor. The slope of the current–voltage curve represents the resistance of the carbon resistor. (B) Calibration plot of the relative change in resistance as a function of the change in temperature.

Sensor calibration

We calibrated the paper-based force sensors using a precision balance and a *LCR* (*L*: inductance, *C*: capacitance, and *R*: resistance) meter (model 885, BK Precision). Fig. 4A shows the experimental output of the sensor (*i.e.*, the change in resistance) as a function of the input to the sensor (*i.e.*, the force applied to the free end of a paper beam) when the carbon resistor was under compressive strain. The resistance changes linearly with the applied force. Based on the calibration curve (Fig. 4A), the range of force measurement was determined to be ±16 mN, and the resolution of force measurement (detection limit) was 0.35 mN (corresponding to the detection limit of the *LCR* meter: 0.1 Ω). The sensitivity of the sensor (*i.e.*, the slope of the curve of linear regression in Fig. 4A) was 0.29 Ω mN^{-1}. With the current experimental system, the resolution of force measurement was primarily limited by the resolution of the resistance measurements (0.1 Ω) obtained using the *LCR* meter. Using a high-resolution *LCR* meter, or integrating a signal-processing circuit to read the change in resistance more accurately, would increase the resolution of force measurement.

Interestingly, and for reasons that remain unclear, the force sensor showed a nonlinear response (Fig. S2†) when the carbon resistor was stretched rather than compressed. Second-order polynomial equations fitted the experimental data well ($R^2 > 0.99$). Since a linear sensor response is desired in most force-sensing applications, we opted only to test and use the

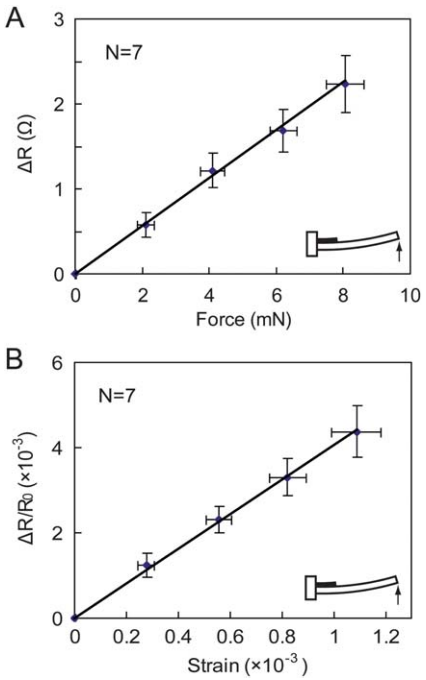

Fig. 4 Calibration of the paper-based force sensor when the carbon resistor is under compressive strain. (A) Calibration plot of the output of the sensor (resistance change) as a function of the input to the sensor (applied force). The solid line represents a linear fit to the experimental data with a regression equation: $y = 0.27x$ ($R^2 = 0.998$, $N = 7$). The slope of the solid line represents the sensitivity of the sensors. (B) Calibration plots of the relative change in resistance as a function of the applied strain. The solid line represents a linear fit to the experimental data with a regression equation: $y = 4.1x$ ($R^2 = 0.998$, $N = 7$). The slope of the solid line represents the gauge factor of the sensor, which is defined as the ratio of relative change in resistance ($\Delta R/R_0$) to the applied mechanical strain (ε).

paper-based sensor in the mode that places the carbon resistor under compressive strain (which we call 'compressive mode'). We collected all the experimental results in the rest of this paper by operating the sensor in the compressive mode.

We calculated the "gauge factor" of the piezoresistive sensor; the gauge factor is defined as the ratio of relative change in resistance of the resistor ($\Delta R/R_0$) to the applied mechanical strain (ε). A higher gauge factor indicates higher sensitivity for the sensor. Fig. 4B shows that the relative resistance changed linearly with the applied strain; the gauge factor was 4.1.

We also quantified the reproducibility of the performance of paper-based sensors with and without silanization by calibrating a sensor seven times. Fig. S3† shows the calibration data collected from an un-silanized sensor (Fig. S3A†) and a silanized sensor (Fig. S3B†). The silanized sensor generated more reproducible output than the un-silanized sensor, probably because the silanization of paper surface minimizes the effect of environmental humidity on the output (change in resistance) of the sensor.

Folding of the paper cantilever

One characteristic of the paper not shared by silicon or quartz is that paper can be folded into three-dimensional structures; this characteristic makes it straightforward to increase the stiffness of the paper sensor while keeping it light. We demonstrated the folding of a paper cantilever beam with the same dimensions as the ones we tested above. As shown in Fig. 5A, we made dashed fold lines on the paper cantilever beam using a laser cutter, and folded the beam to form a wedge-shaped structure (Fig. 5B) that

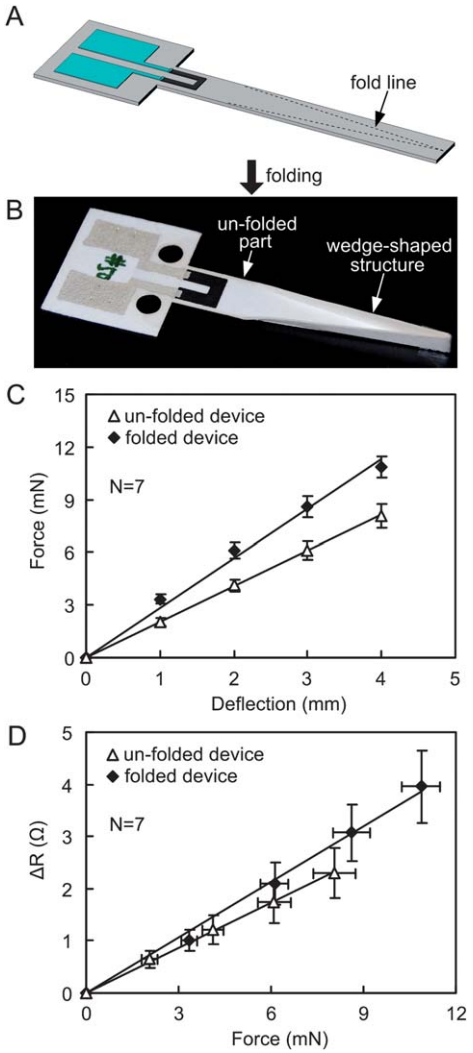

Fig. 5 Folding of the paper cantilever beam increases stiffness of the beam and the sensitivity of the sensor. (A) Schematic diagram of a paper cantilever beam with perforation of the fold lines made by a laser cutter. (B) A photograph of a folded sensor with a wedge-shaped structure. (C) Force–deflection curves of the folded and un-folded beams. The solid lines represent linear fits to the experimental data with regression equations: $y = 2.0x$ ($R^2 = 0.9998$, $N = 7$) for un-folded devices, and $y = 2.8x$ ($R^2 = 0.991$, $N = 7$) for folded devices. The stiffness (2.8 mN mm^{-1}) of the folded beams is 40% higher than that of the un-folded beams (2.0 mN mm^{-1}). (D) Calibration plots of output of the sensor (change in resistance) as a function of input of the sensor (force applied to the free end of the beam). The solid lines represent linear fits to the experimental data with regression equations: $y = 0.36x$ ($R^2 = 0.996$, $N = 7$) for un-folded devices, and $y = 2.9x$ ($R^2 = 0.998$, $N = 7$) for folded devices. Because the folding of the beam concentrates mechanical strain on the carbon resistor, the sensor with a folded beam showed higher sensitivity (0.36 Ω mN^{-1}) than the sensor with an un-folded beam (0.29 Ω mN^{-1}).

is stiffer than the un-folded part of the beam. This folding enhanced the stiffness of the cantilever beam without increasing the weight of the beam. Fig. 5C shows the force–deflection curves of the folded and un-folded beams ($N = 7$); the stiffness (2.8 mN mm^{-1}) of the folded beam is 40% higher than that of the un-folded beam (2.0 mN mm^{-1}). The folding of the cantilever beam concentrated mechanical strain on the carbon resistor, and thus increased the sensitivity of the sensor. Fig. 5D shows calibration plots of the output (change in resistance) of the folded sensor as a function of the input (force applied to the free end of the beam) to the sensor. The sensitivity of the folded sensors was 0.36 Ω mN^{-1}; this value is 24% higher than the sensitivity (0.29 Ω mN^{-1}) of the un-folded sensors.

Monolithic integration of a signal-processing circuit onto the paper device

In order to convert the change in resistance of the sensor into a more readable electrical signal (voltage), a Wheatstone bridge circuit (Fig. 6A) is commonly used for signal processing in MEMS piezoresistive sensing systems. There are two ways in conventional MEMS to integrate signal-processing circuits with the MEMS sensor: (i) a two-chip approach, where a MEMS device is mounted on a printed circuit board (PCB) on which the signal processing circuit is laid out; the electrical connection is achieved using wire-bonding.[14] (ii) A monolithic approach, where a MEMS device and a conventional IC signal processing circuit (*e.g.*, complementary metal oxide semiconductor—CMOS) are microfabricated on the same silicon chip (*e.g.*, CMOS–MEMS).[15] The monolithic approach provides a smaller footprint for the chip, and much lower noise levels, but is more complicated to fabricate.

For our paper-based MEMS sensors, we developed a monolithic approach that integrated the Wheatstone bridge circuit with the paper-based sensor. This approach was inspired by a previous paper,[16] which used paper as a flexible PCB for construction of circuits. We laid out connections of the entire Wheatstone bridge circuit (including the carbon resistor R_s in Fig. 6B) by screen-printing silver ink on the base of the paper-based sensor, then gluing three surface-mount resistors (R_1, R_2, R_3) at appropriate locations, and finally 'soldering' them into the circuit using silver ink. R_3 is an adjustable resistor that is used to initially balance the Wheatstone bridge.

Fig. 6C illustrates a calibration curve of the paper-based sensor with an integrated Wheatstone bridge circuit. The resolution of the force measurement was improved to 120 μN (corresponding to a voltage detection limit of 0.1 mV). The sensitivity of the sensor after integrating a Wheatstone bridge circuit was 0.84 mV mN^{-1}.

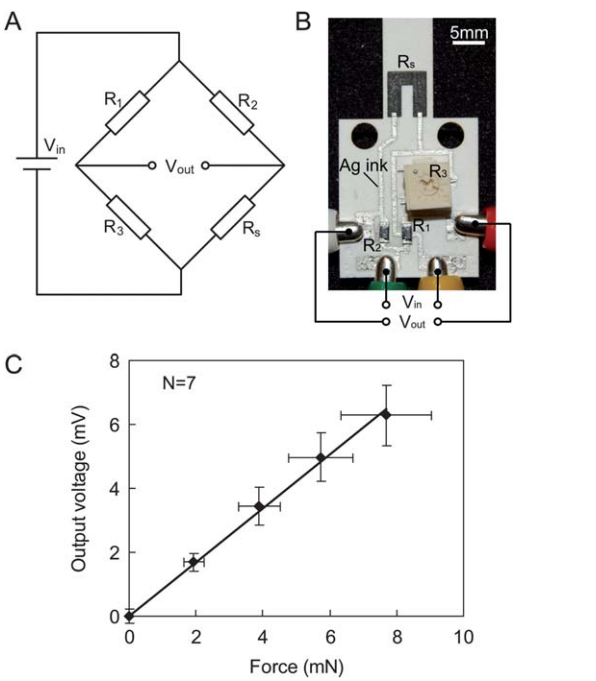

Fig. 6 Monolithic integration of a Wheatstone bridge circuit with the paper-based sensor. (A) Schematic diagram of a Wheatstone bridge circuit, where R_s is the resistor with unknown resistance to be measured and R_1, R_2, and R_3 are resistors with known resistance. (B) A photograph of a Wheatstone bridge circuit laid out on the base of a paper-based force sensor. Electrical connections were screen-printed using silver ink to connect the four resistors. (C) Calibration plot of the output of the circuit as a function of the input to the sensor (force applied to the free end of the sensor beam). The solid line represents a linear fit to the experimental data with a regression equation: $y = 0.84x$ ($R^2 = 0.996$, $N = 7$).

Comparison of the paper-based sensor with a commercial silicon-based MEMS sensor

Table 1 lists specifications of a commercial MEMS silicon force sensor (AE-801, Kronex Technology, specifications provided by the manufacturer) and our paper-based force sensor; both sensors are based on piezoresistive sensing. The commercial sensor is manufactured in silicon using standard microfabrication technology. Because the Young's modulus of the paper is much lower than silicon, the paper-based MEMS sensor has a low natural resonant frequency (~25 Hz); this value indicates that the paper-based sensor could be used only for detection of low frequency or static forces. The paper-based sensor has a lower force measurement range, resolution, and sensitivity than the commercial silicon-based sensor, but it has low cost, and requires only simple fabrication. In terms of fabrication and cost, the paper-based sensor may provide a simpler and less expensive solution for some force sensing applications than a silicon-based sensor: silicon and paper based MEMS will probably be complementary rather than competitive technologies.

Applications

After testing the device performance, we applied the paper-based force sensor to characterization of the mechanical properties of a soft material. Soft materials, such as polydimethylsiloxane (PDMS) and polyacrylamide (PAA), have been widely used for constructing micro-devices[17–20] and in studies of mammalian cell culture.[21] Mechanical properties (*e.g.*, Young's modulus) of soft materials are important in applications where the soft material serves as mechanical components (*e.g.*, microfluidic valves/pumps[22] and force sensing posts[17–20]) or cell culture substrates (the stiffness of which affects the surface chemistry of the

Table 1 Comparison of specifications of a commercial silicon-based MEMS sensor (AE-801, Kronex Technology) and our paper-based MEMS sensor

Specifications	Commercial silicon MEMS sensor (AE-801, Kronex)	Paper-based MEMS sensor
Sensing principle	Piezoresistive	Piezoresistive
Material	Silicon	Paper, carbon/silver inks
Beam size ($L \times W \times H$)	5 mm × 1 mm × 0.75 mm	44.5 mm × 7.7 mm × 0.34 mm
Beam stiffness	2000 mN mm^{-1}	2 mN mm^{-1}
Natural frequency	~12 kHz	~25 Hz
Force range	120 mN	16 mN
Force resolution	40 μN	120 μN
Sensitivity	2.5 mV mN^{-1}	0.84 mV mN^{-1}
Fabrication process	>1 day in cleanroom	<1 hour in laboratory
Device cost	$168 per device (commercial price)[a]	$0.04 per device (cost of materials for a prototype)

[a] This price consists of, in addition to profit margin, a wide variety of costs, including materials, amortization and operation of facilities, packaging, quality control, marketing and distribution, and so on.

material, and the behavior of the cells[21]). Characterization of the mechanical properties of soft materials is based primarily on tensile testing and nanoindentation, both of which require access to expensive equipments. We demonstrated that our paper-based force sensor can be used to measure the Young's modulus of PDMS.

We prepared PDMS cantilever beams by cutting appropriately sized slabs from a sheet using a scalpel, and then controlled a paper-based force sensor to deflect the cantilever beam (Fig. 7A, the dimensions of the beams are summarized in Table S2†). During deflection, we measured the applied contact forces and resultant deflections of the cantilever beam. The Young's modulus of the PDMS was calculated using eqn (1). The time required to complete measurements with one cantilever beam was <5 minutes.

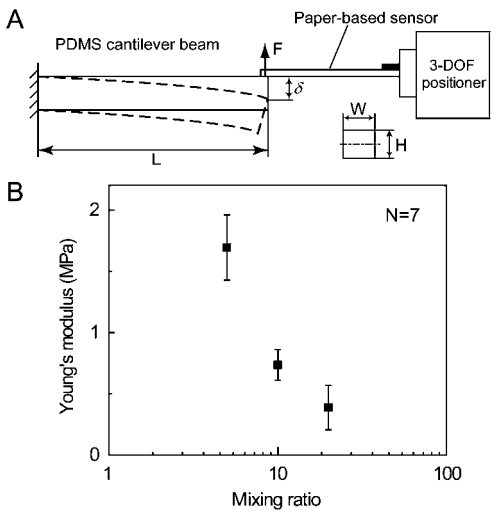

Fig. 7 Mechanical characterization of PDMS using a paper-based force sensor. (A) Schematic diagram of the setup for measuring the Young's modulus of PDMS cantilever beams. A paper-based force sensor is controlled to contact and deflect a PDMS cantilever beam, during which the contact force and deflection of the PDMS beam are measured. The Young's modulus of the PDMS is calculated using a beam equation. The dimensions of the PDMS beams are summarized in Table S2†. (B) A plot of measured values of Young's modulus for PDMS with different mixing ratios (w/w: 5 : 1, 10 : 1, and 20 : 1) of the polymer base to the cross-linking agent. The values of Young's modulus in the plot are means of data from seven beams.

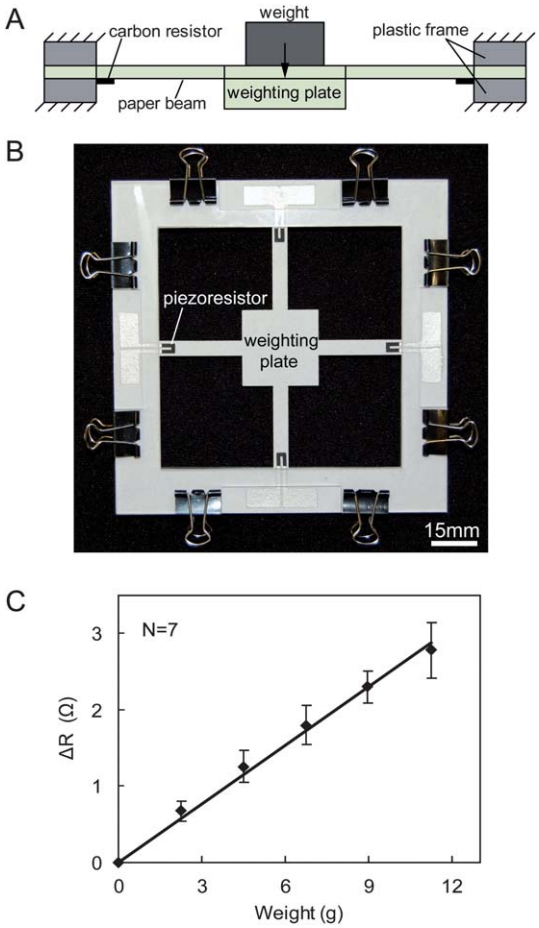

Fig. 8 A paper-based weighing balance. (A) A schematic side view of a paper-based balance where force-sensing beams with carbon resistors are used for tethering a weighing plate, and measuring the force due to gravity of a weight. (B) A photograph of the paper-based balance where four force sensing beams are involved. (C) Calibration plot of the resistance change from one sensing beam as a function of applied calibration weight. The solid line represents a linear fit to the experimental data with a regression equation: $y = 0.26x$ ($R^2 = 0.993$, $N = 7$).

We tested three types of PDMS with different levels of cross-linking (mixing ratios (w/w) of the polymer base to the cross-linking agent: 5 : 1, 10 : 1, and 20 : 1). PDMS is supplied in two components: the un-cross-linked elastomer (polymer base) and the cross-linking agent. By varying the ratio (w/w) of the polymer base to the cross-linking agent, we changed the level of inter-chain cross-linking, and generated samples of PDMS with different stiffnesses (the stiffness decreases in the order: polymer base : cross-linker = 5 : 1 > 10 : 1 > 20 : 1). The experimental results (Fig. 7B) agree with the data in the literature.[23,24]

We also developed a paper-based weighing balance using the same piezoresistive sensing principle. As shown in Fig. 8A, paper-based force-sensing beams were used to tether a weighing plate and measure forces due to the gravity of an object placed on top of the weighing plate. Fig. 8B is the photograph of a balance prototype, where four force-sensing beams are involved. We calibrated the balance by measuring the change in resistance of the carbon resistor from one sensing beam as a function of the applied weight (Fig. 8C). The measurement range of the balance was 15 g, and the resolution of the measurement was 0.39 g.

Conclusions

We explored the feasibility of fabricating MEMS sensors using paper as the structural material, and developed paper-based piezoresistive force sensors. The use of paper for construction of MEMS significantly simplifies the fabrication process relative to that used for silicon, and eliminates the requirement of cleanroom facilities; this simplification comes, of course, with a significant decrease in certain elements of performance (especially the frequency of response). We also demonstrated folding of the paper cantilever beam of the sensor to increase the stiffness of the beam, and to improve the sensitivity of the sensor. To minimize the effect of humidity on the paper-based sensor, we made the paper surface hydrophobic by silanizing it with a fluorohydrocarbon; silanization of the paper surface improved the performance of the sensor, and decreased its sensitivity to environmental factors such as humidity. The paper-based sensor presented in this paper is suitable for force sensing applications that require moderate sensing capabilities, operation in a limited range of temperatures, and consideration of device cost.

The paper-based MEMS technology has six advantages. (i) It represents a simple, fast, and low-cost solution for the problem of constructing low-cost MEMS devices. (ii) Paper, as the major material for device construction, is readily available, lightweight, and easy to manufacture (that is, there are highly developed technologies for cutting and folding it). (iii) Paper can be folded into three-dimensional structures with high stiffness and anisotropic responses but lightweight; there is no corresponding capability for folding of silicon. (iv) Manufacturing of paper-based MEMS devices has the potential to be fairly simple and to involve low-cost tooling; prototyping can be carried out using very simple tools, does not require access to cleanroom, and has the potential for mass production (by automatic paper cutting and screen printing). (v) Paper can also be used as a substrate for laying out simple electrical circuits, and permits electrical circuits for signal processing to be readily integrated with the paper-based sensor to form monolithic paper-based chips. (vi) The versatile chemistries available to modify the surface of paper, and its high ratio of surface area to weight, offer opportunities for surface tailoring to generate new types of sensitivities.

The paper-based MEMS force sensor has several limitations, of which three are: (i) it has lower sensing performance (*i.e.*, measurement range, resolution, and sensitivity) than the silicon-based force sensor. (ii) Because paper has a lower Young's modulus (2 GPa) than silicon (130–170 GPa), it has a low natural resonant frequency (~25 Hz), and is therefore limited to low frequency or static measurement of forces. (iii) Although we have not explicitly examined a full range of environmental factors, paper-based MEMS will be more sensitive than silicon-based devices to high temperatures, atmospheric components (*e.g.*, water vapor, ozone, prolonged exposure to dioxygen or peroxides); these sensitivities may, of course, also become advantages in some contexts.

Acknowledgements

This work was supported by the Bill & Melinda Gates Foundation (#51308), the Defense Advanced Research Projects Agency (DARPA) N/MEMS S&T Fundamentals Program under grant No. N66001-1-4003 issued by the Space and Naval Warfare Systems Center Pacific (SPAWAR) to the Micro/nano Fluidics Fundamentals Focus (MF3) Center, and postdoctoral fellowships from the Natural Sciences and Engineering Research Council of Canada (to X.Y.L. and X.J.L.) and NanoScience and Engineering Center (to M.M.). We thank Tiefeng Li for helpful discussions.

References

1 A. C. R. Grayson, R. S. Shawgo, A. M. Johnson, N. T. Flynn, L. I. Yawen, M. J. Cima and R. Langer, *Proc. IEEE*, 2004, **92**, 6–21.
2 C. Liu, *Adv. Mater.*, 2007, **19**, 3783–3790.
3 K. D. Wise, *Sens. Actuators, A*, 2007, **136**, 39–50.
4 D. H. Kim, P. K. Wong, J. Park, A. Levchenko and Y. Sun, *Annu. Rev. Biomed. Eng.*, 2009, **11**, 203–233.
5 K. E. Petersen, *Proc. IEEE*, 1982, **70**, 420–457.
6 A. W. Martinez, S. T. Phillips, M. J. Butte and G. M. Whitesides, *Angew. Chem., Int. Ed.*, 2007, **46**, 1318–1320.
7 A. W. Martinez, S. T. Phillips, G. M. Whitesides and E. Carrilho, *Anal. Chem.*, 2010, **82**, 3–10.
8 X. Li, J. Tian, T. Nguyen and W. Shen, *Anal. Chem.*, 2008, **80**, 9131–9134.
9 R. Pelton, *TrAC, Trends Anal. Chem.*, 2009, **28**, 925–942.
10 M. A. Nash, J. M. Hoffman, D. Y. Stevens, A. S. Hoffman, P. S. Stayton and P. Yager, *Lab Chip*, 2010, **10**, 2279–2282.
11 Z. Nie, F. Deiss, X. Y. Liu, O. Akbulut and G. M. Whitesides, *Lab Chip*, 2010, **10**, 3163–3169.
12 N. Inagaki, *Plasma Surface Modification and Plasma Polymerization*, Technomic Publishing Company, Lancaster, Pennsylvania, 1996.
13 L. Gao and T. J. McCarthy, *Langmuir*, 2008, **24**, 9183–9188.
14 K. Kim, X. Y. Liu, Y. Zhang and Y. Sun, *J. Micromech. Microeng.*, 2008, **18**, 055013.
15 H. Baltes, O. Brand, A. Hierlemann, D. Lange and C. Hagleitner, in *Proc. IEEE Conf. Micro Electro Mechanical Systems*, 2002, pp. 459–466.
16 A. C. Siegel, S. T. Phillips, M. D. Dickey, N. Lu, Z. Suo and G. M. Whitesides, *Adv. Funct. Mater.*, 2010, **20**, 28–35.
17 J. L. Tan, J. Tien, D. M. Pirone, D. S. Gray, K. Bhadriraju and C. S. Chen, *Proc. Natl. Acad. Sci. U. S. A.*, 2003, **100**, 1484–1489.
18 X. Y. Liu, Y. Sun, W. H. Wang and B. M. Lansdorp, *J. Micromech. Microeng.*, 2007, **17**, 1281–1288.
19 Y. Zhao and X. Zhang, *Sens. Actuators, A*, 2006, **125**, 398–404.
20 X. Y. Liu, R. Fernandes, A. Jurisicova, R. F. Casper and Y. Sun, *Lab Chip*, 2010, **10**, 2154–2161.

21 X. Q. Brown, K. Ookawa and J. Y. Wong, *Biomaterials*, 2005, **26**, 3123–3129.
22 M. A. Unger, H. P. Chou, T. Thorsen, A. Scherer and S. R. Quake, *Science*, 2000, **288**, 113–116.
23 D. Armani, C. Liu and N. Aluru, in *Proc. IEEE Conf. Micro Electro Mechanical Systems*, 1999, pp. 222–227.
24 A. Mata, A. Fleischman and S. Roy, *Biomed. Microdevices*, 2005, **7**, 281–293.

